Journal of Solid State Chemistry **168,** 208–216 (2002)
doi:10.1006/jssc.2002.9712

Electrical Behavior of New Orthophosphates $Na_2M_3(PO_4)_3$ ($M_3 = GaMn_2$, $GaCd_2$, $InMn_2$ and FeMnCd) with Alluaudite-Like Structure

C. Durio,* A. Daidouh,*,[1] N. Chouaibi,† C. Pico,* and M. L. Veiga*

*Departamento de Química Inorgánica I, Facultad de Ciencias Químicas, Universidad Complutense, 28040 Madrid, Spain; and †Département de Chimie, Faculté des Sciences de Tetouan, Université Abdelmalek Essaidi, Tetouan, Morocco

Received March 28, 2002; in revised form July 8, 2002; accepted July 16, 2002

New sodium orthophosphates of general formula $Na_2M_3(PO_4)_3$ belonging to the alluaudite-type structure have been synthesized and characterized by neutron and X-ray powder diffraction. The nature of the M_3 elements ($M_3 = GaMn_2$, $GaCd_2$, $InMn_2$ and FeMnCd) was chosen in order to analyze their influence on electrical and magnetic properties. The conductivity of these materials was measured by the complex impedance method and the transport mechanism was studied from complex permittivities and modulus formalism. Electrical results including charge/discharge experiments showed two main behaviors: $GaCd_2$ and FeMnCd behave as purely ionic conductors whereas $GaMn_2$ and $InMn_2$ are mixed ionic–electronic conductors. The magnetic susceptibility data reveal the antiferromagnetic behavior of FeMnCd, $InMn_2$ and $GaMn_2$, with a weak ferromagnetic transition at low temperatures.

Key Words: **orthophosphates; alluaudite structure; electrical conductivity; antiferromagnetic behaviour.**

INTRODUCTION

The structural features of oxosalts of composition $X_2M_3(EO_4)_3$ (E = P, As) belonging to the alluaudite structure type are extensively studied, since they are versatile materials that can tolerate a wide range of compositional variation. At the same time, they can exhibit interesting electric and/or magnetic properties due to the presence of mobile cations located along the tunnels and transition metal cations that share edges, respectively. However, metal orthophosphates with this structural type are scarcely studied up till now.

The alluaudite structure, which is found in natural minerals, was reported first by Fisher in 1955 (1) and then studied by Moore in 1971 (2). The general crystallochemical formula proposed for isomorphous phases was $X(2)X(1)M(1)M(2)(PO_4)_3$, in which X and M cations are written according to decreasing size. Thus, the X sites can be occupied by medium-sized cations with low charge (in general monovalent in $X(1)$ and divalent in $X(2)$ such as Na^+ and Ca^{2+}, respectively) and the M sites can locate six-fold coordinated transition cations. In the latter, coordination polyhedra are very distorted for $M(1)$ (e.g., Mn^{2+} or Fe^{2+}) and are nearly regular octahedra for $M(2)$, usually smaller than the previous ones (e.g., Al^{3+} or Fe^{3+}). Nevertheless, some degree of disorder is very frequently encountered with respect to the ideal cation distribution (3, 4).

Recently, we have reported the structure, magnetism and Mössbauer spectra of $Ag_2FeMn_2(PO_4)_3$ (5) and the ionic conductivity of $(Ag_{1-x}Na_x)_2FeMn_2(PO_4)_3$ with $x = 0$, 0.5, and 1 (6). The alluaudite structure of both systems, deduced from room-temperature neutron diffraction measurements, allowed us to improve the distribution of the transition metals (Fe, Mn) along the edge-sharing MnO_6–FeO_6–MnO_6 octahedra, concluding that the cations Mn and Mn/Fe are located, respectively, in 4*e* and 8*f* positions. The magnetic susceptibility measurements showed a weakly ferromagnetic state below 19 K that may be due to intrinsic canting of an antiferromagnetically coupled lattice. The Mössbauer spectral parameters confirmed the presence of only Fe(III) in the octahedral sites. Finally, the ionic conductivity study revealed that the silver compound is a better conductor and showed lower activation energy than the sodium derivative.

In the present work, we report the synthesis and structure of a new series of sodium alluaudite orthophosphates. We have extended the study of the electrical conductivity in these solid electrolytes, that contain main

[1] To whom correspondence should be addresssed. Fax: +34 91 394 43 52. E-mail: daidouh@quim.ucm.es.

0022-4596/02 $35.00

and transition elements, in order to clarify the influence of the unit-cell size and the electronic configuration of such elements on the cation mobility and the possible electronic contribution. At the same time, we carried out the magnetic study of these materials. Other related phases in which the charge carriers are Ag^+ cations will be reported in due course.

EXPERIMENTAL

Synthesis

The chemicals used were commercial $NaNO_3$ (Merck), Ga_2O_3 (Merck), In_2O_3 (Merck), $Fe(NO_3)_3 \cdot 9H_2O$ (Panreac), $Cd(NO_3)_2$ (Merck), $Mn(C_5O_2H_7)_2$ (Aldrich) and $(NH_4)_2HPO_4$ (Panreac) and all of them were about 99% pure. Stoichiometric amounts of starting reagents were well mixed in an agate mortar and were preheated at 723 K to eliminate gaseous materials. Then, the powders were calcined progressively between 973 and 1173 K for 24 h in air with several intermediate grindings. The resulting powders, $Na_2GaMn_2(PO_4)_3$ (violet), $Na_2GaCd_2(PO_4)_3$ (white), $Na_2InMn_2(PO_4)_3$ (white-violet) and $Na_2FeMnCd(PO_4)_3$ (brown) were microcrystalline pure monophases in all cases.

X-Ray and Neutron Diffraction

Phase purity analysis and structure determination was carried out by X-ray diffraction with a Phillips X'pert MPD diffractometer and a PW 3050/00 goniometer, using Ni-filtered, Cu$K\alpha$ radiation and 2θ step scan of 0.04° with a counting time of 12 s for each step. The goniometer was connected to a PC controlled by the commercial program PC-APD (Analytical Powder Diffraction software, 4·0).

Neutron powder diffraction data for $Na_2FeMnCd(PO_4)_3$ were recorded at room temperature on the D1A high-resolution powder diffractometer ($\lambda = 1 \cdot 9110$ Å) at the Institute Laue-Langevin (Grenoble, France).

Both neutron and X-ray patterns were analyzed by the Rietveld method (Fullprof program (12)). A pseudo-Voigt function was chosen to generate the lineshape of the diffraction peaks. The background was estimated by linear interpolation between points corresponding to regions without reflections.

Electrical Measurements

For electrical measurements, pellets 12 mm in diameter and about 1.5 mm thickness were prepared by pressing fine powders at 5 t/cm^2. The pellets were sintered at 1073 K for 24 h in order to increase their mechanical strength. After these treatments, the samples achieved about 85% of theoretical density. For blocking electrodes, Pt paint was coated on both faces of the pellets and was cured at 973 K for 6 h to remove the volatile organic matter.

Impedance measurements using Pt electrodes were carried out over the frequency range from 10^7 to 1 Hz between 303 and 873 K using a Solartron SI 1260 Gain-Phase Analyser connected to a PC computer. The amplitude of the dc signal applied across the samples was less than 100 mV. Results were reproducible within less than 8%. Polarization measurements in dc were carried out with the same pellets used in ac experiments. The measurements were performed for all the samples at 723 K and with a charging voltage of 0.5 V. The equipment includes a standard resistor that was in series with the sample during the charging and discharging cycles.

Magnetic Measurements

Magnetic properties were performed with a Quantum design SQUID magnetometer. The temperature dependence of susceptibilities was registered at decreasing temperatures from 300 to 2 K at an applied field of 0.5 T.

RESULTS AND DISCUSSION

Structural Characterization

X-ray diffraction patterns demonstrate that the room-temperature crystal structure of the title compounds is similar to that previously reported in many papers (7–11) and it is alluaudite-like belonging to the monoclinic space group $C2/c$. The unit cell constants and volumes derived from Fullprof refinements (12) are summarized in Table 1.

Further study of the structure by means of neutron diffraction was carried out for the $Na_2FeMnCd(PO_4)_3$ compound, as it contains three different transition metals (Fe, Mn, Cd), and the distribution of them along the $(FeMnCdO_{12})_\infty$ chains cannot be determined by using only X-ray diffraction refinements, due to their nearly identical X-ray scattering power. Neutron diffraction results allowed to improve our previous model and the accurate agreement between the final observed, calculated and difference diffraction profiles is seen in Fig. 1. The refinement yielded the parameters listed in the right-hand side column of Table 1 and the Fe, Mn and Cd atoms were fixed in the positions cited in Table 2. Some representative bond lengths and angles are listed in Table 3.

From the above results, we can conclude that all the $Na_2M_3(PO_4)_3$ phases are isostructural and only show small variations in the unit-cell parameters that agree well with the respective ionic radii. They are denoted in the following discussion with the corresponding M_3 metal symbols of the formula, i.e., $GaMn_2$, $GaCd_2$, $InMn_2$ and FeMnCd.

TABLE 1
Crystallographic Data for $Na_2GaMn_2(PO_4)_3$, $Na_2InMn_2(PO_4)_3$, $Na_2GaCd_2(PO_4)_3$ and $Na_2FeMnCd(PO_4)_3$ Obtained from X-Ray and Neutron Diffractions (*)

Parameters	GaMn2	InMn2	GaCd2	FeMnCd	FeMnCd(*)
1. *Structure parameters*					
A (Å)	12.019(4)	12.248(1)	12.188(3)	12.169(5)	12.1687(3)
B (Å)	12.559(2)	12.823(4)	12.799(1)	12.685(3)	12.6842(4)
C (Å)	6.495(5)	6.607(2)	6.547(3)	6.524(4)	6.5250(3)
β (°)	114.63(3)	114.97(3)	114.75(2)	114.51(2)	114.518(4)
V (Å^3)	891.19(3)	940.64(4)	926.44(2)	916.32(3)	916.32(2)
2. *Structure solution and refinement*					
R_P	15.6	16.7	15.4	16.1	9.2
R_{WP}	19.0	19.9	18.1	18.3	8.8
R_B	8.9	6.9	8.7	11.9	3.3
R_F	6.1	5.3	6.2	8.4	3.2
χ^2	11.3	6.3	11.3	7.0	2.1
Reflections	1327	1398	1376	1361	1361

Note. Refined parameters: 56.

Electrical Conductivity

Impedance spectroscopy. Impedance spectroscopy is often used to analyze separately the bulk, grain boundary and electrode processes of polycrystalline ceramic materials showing ionic or mixed conductivity (13). This method has been widely used to assess whether resistant grain boundaries may spoil the conductivity of solid electrolytes and has also been used to study other materials with useful grain boundary properties (14).

Cole–Cole plots (15) of the $GaMn_2$, $GaCd_2$ and $InMn_2$ specimens showed a semicircle at high frequencies and a spike ($GaCd_2$) or a big incomplete semicircle ($GaMn_2$ and $InMn_2$) in the low-frequency region (Fig. 2a), suggesting that resistance of the grain boundary would be fairly small, and therefore the electrode process is less likely to affect the bulk or intragranular mechanism (16). In fact, the major component was the first large semicircle which could be assumed to be the bulk resistance and from which the electrical conductivity is deduced. The semicircular features of these three materials are nearly identical, so henceforth the curves will be presented for only one of them, taking as an example those of the $GaCd_2$ compound.

By contrast, the impedance behavior of the FeMnCd material is somewhat different, and the data seem to define two semicircles at high and medium frequencies and a spike at low frequency range (Fig. 2b). The first semicircle is attributed to an intragranular process, the second one to an

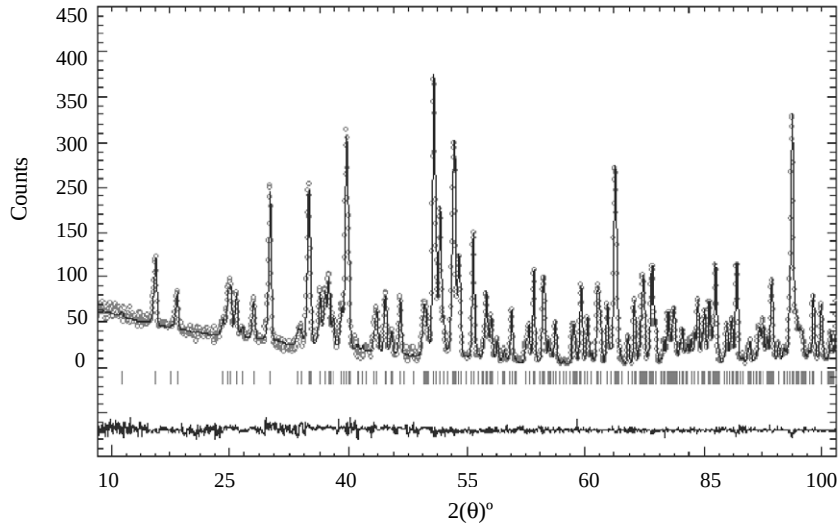

FIG. 1. Observed (circles), calculated (solid lines) and difference (bottom) neutron diffraction profiles for $Na_2FeMnCd(PO_4)_3$.

TABLE 2
$Na_2FeMnCd(PO_4)_3$ Positional Parameters and Equivalent Isotropic Temperature Factors Obtained from Neutron Diffraction

Atom	Site	*x*/*a*	*y*/*b*	*z*/*c*	*B*iso(Å)2
Na(1)	4b	0	$\frac{1}{2}$	0	1.72(3)
Na(2)	4e	0	–0.015(3)	$\frac{1}{4}$	1.97(2)
Cd	4e	0	0.273(0)	$\frac{1}{4}$	1.54(5)
Mn/Fe	8f	0.274(2)	0.655(1)	0.362(2)	1.34(1)
P(1)	4e	0	–0.284(5)	$\frac{1}{4}$	0.59(2)
P(2)	8f	0.247(2)	–0.103(3)	0.132(3)	0.67(2)
O(1)	8f	0.459(5)	0.707(2)	0.548(2)	1.29(8)
O(2)	8f	0.085(3)	0.623(0)	0.271(2)	1.09(7)
O(3)	8f	0.317(2)	0.665(1)	0.091(4)	1.23(8)
O(4)	8f	0.113(4)	0.400(4)	0.296(3)	1.16(9)
O(5)	8f	0.236(5)	0.815(5)	0.295(3)	1.10(7)
O(6)	8f	0.330(1)	0.497(1)	0.384(1)	1.07(7)

intergranular response, and the spike to the electrode process occurring at the material/electrode interface (16). It is well known that the grain boundary behavior of polycrystalline materials often deviates from a simple brick layer approximation (17), especially for materials with broad grain size distribution, irregular grain shapes, etc.

TABLE 3
Selected Bond Distances (Å) and Angles (deg) for $Na_2FeMnCd(PO_4)_3$

Na (1)–O(2)	2.261(5) × 2		
Na (1)–O(2)	2.650(3) × 2	Na (2)–O(1)	2.719(5) × 2
Na (1)–O(2)	2.239(1) × 2	Na (2)–O(6)	2.561(2) × 2
Na (1)–O(4)	2.598(4) × 2	Na (2)–O(6)	2.435(4) × 2
Mean	*2.437*	*Mean*	*2.572*
Cd–O(1)	2.356(3) × 2	*M*–O(1)	2.164(4) × 2
Cd–O(3)	2.449(2) × 2	*M*–O(2)	2.163(3) × 2
Cd–O(4)	2.054(4) × 2	*M*–O(3)	2.045(5) × 2
Mean	*2.286*	*M*–O(5)	2.095(3) × 2
		M–O(5)	2.323(3) × 2
P(1)–O(1)	1.545(1) × 2	*M*–O(6)	2.098(2) × 2
P(1)–O(2)	1.542(3) × 2	*Mean*	*2.148*
Mean	*1.543*		
		O(3)–P2–O(4)	110.661(2)
P(2)–O(3)	1.548(5)	O(3)–P2–O(5)	98.836(1)
P(2)–O(4)	1.577(1)	O(3)–P2–O(6)	107.451(1)
P(2)–O(5)	1.531(4)	O(4)–P2–O(5)	101.883(3)
P(2)–O(6)	1.553(5)	O(4)–P2–O(6)	123.217(2)
Mean	*1.552*	O(5)–P2–O(6)	112.074(2)
O(1)–P1–O(1)	101.935(1)		
O(1)–P1–O(2)	121.896(2)		
O(1)–P1–O(2)	115.991(2)		
O(2)–P1–O(2)	79.750(4)		

Note. M = Fe/Mn

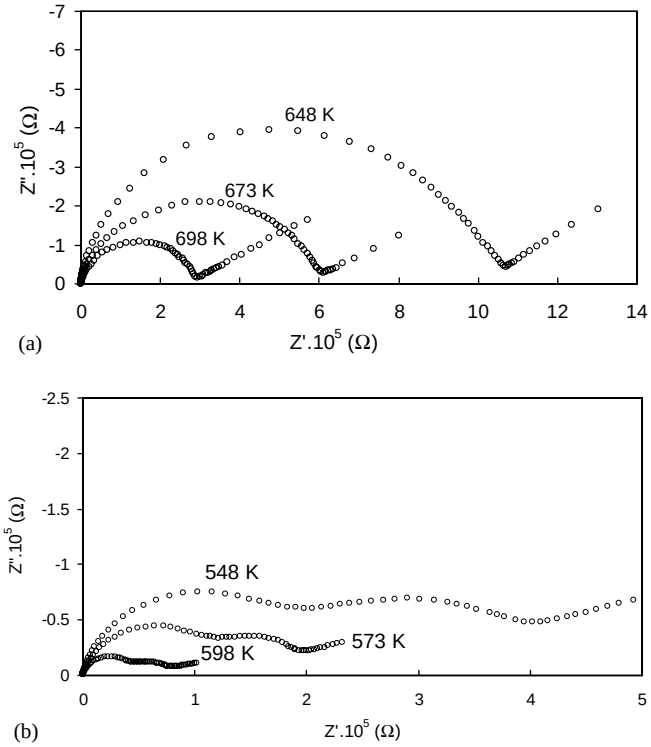

FIG. 2. Complex impedance plots for (a) $Na_2GaCd_2(PO_4)_3$ and (b) $Na_2FeMnCd(PO_4)_3$.

The equivalent circuit used to fit the complex impedance data of FeMnCd is depicted in Fig. 3. The least-squares fitting model is composed of two circuits of parallel *RC* elements connected in series corresponding, respectively, to bulk and grain boundaries electrode responses. The additional constant phase elements (CPEs) were used to give the largest coverage of the semicircles fitting, and then the level of agreement between experiment and simulation is quite satisfactory for the bulk and grain boundary arcs. The low-frequency spike, or the incomplete semicircle, can be assigned to space charge polarization or to the Warburg impedance (18, 19).

A frequency dependence of electrical conductivity for $GaCd_2$ is depicted in Fig. 4. Starting from low frequencies, we observe the presence of a wide plateau followed by an increase in conductivity. The plateau characterizes the conduction which is caused mainly by the hopping motion of the mobile ions and determines the dc value of conductivity. Thereafter, the slope of this plateau increases linearly with increasing frequencies. Such a behavior is attributed to the relaxation of the mobile ion hopping, which is due to the Coulomb interactions of the charge carriers and the disorder within the structure (20, 21). Therefore, the ac conductivity results take the form $\sigma(\omega) = \sigma_0 + A\omega^n$, where σ_0 is a dc term, A is a temperature-dependent parameter and n is the slope of the high-frequency data ($0 < n < 1$) (22).

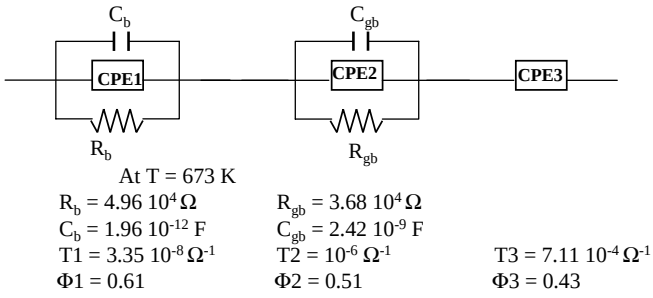

FIG. 3. Equivalent circuit to fit the impedance complex plots of $Na_2FeMnCd(PO_4)_3$. The parameters listed were calculated from the data taken at 673 K.

The frequency dependence of the real part (ε') of the permittivity for $GaCd_2$ and FeMnCd are depicted in Fig. 5. At high frequencies, strong dispersions are observed in both cases, as discussed before, and this behavior is characteristic of interactions between mobile cations when they are in motion. The dispersions observed at medium frequencies in FeMnCd can be assigned to the grain boundary effect. Nevertheless, the imaginary parts (ε'') depicted in Fig. 6 show a –1 slope in all the synthesized compounds, suggesting that they are mainly dominated by the dc conduction mechanism (23, 24).

The modulus formalism is widely used in the analysis of the admittance data because of its relative insensitivity to blocking phenomena. The modulus spectrum of the imaginary component, M'', vs $\log \omega$ for $GaCd_2$ (Fig. 7a) is characterized by a single Debye peak, suggesting that these materials can be interpreted by an equivalent circuit composed of a single parallel RC element. At the same time, the presence of two semicircles in the impedance spectroscopy of FeMnCd can be visualized by the presence of two peak maxima in each measurement (Fig. 7b), suggesting that the bulk behavior and the grain boundary phenomenon are present as separate peaks. In all cases, the normalized peaks are broader than the Debye ones, and this behavior is typical of materials that do not behave as ideal electrolytes (25).

On the other hand, conductivity values plotted against reciprocal temperature are shown in Fig. 8. The relation between specific conductivity and temperature is given by the Arrhenius expression in the form: $\ln \sigma T = \ln \sigma_0 - E_a/RT$, where E_a is the activation energy involved in the transport process, σ_0 is a constant, and R and T are the gas constant and the absolute temperature, respectively. As a general trend, a linear relationship is observed in all the studied compounds. Conductivity data at selected temperatures and activation energies relative to these samples are listed in Table 4.

It was expected (see Fig. 8 and Table 4) that activation energies decrease with increasing unit-cell volumes, and this could be understood in terms of the size relation between the mobile cations and the bottleneck of the diffusion pathway. In this sense, the distortion of the octahedra, estimated from the lattice parameters variations, would contract the bottlenecks and make more difficult for the charge carriers to move between adjacent site vacancies.

It should be pointed out that the sodium atoms are located in the tunnels on two independent sites and that the Na(1) sites have an irregular environment of eight oxygen atoms (Fig. 9a) with Na–O mean distances ranging from ca. 2.40 Å for $GaMn_2$ to 2.50 Å for $InMn_2$. On the other hand, two Na(1) neighboring positions are separated by

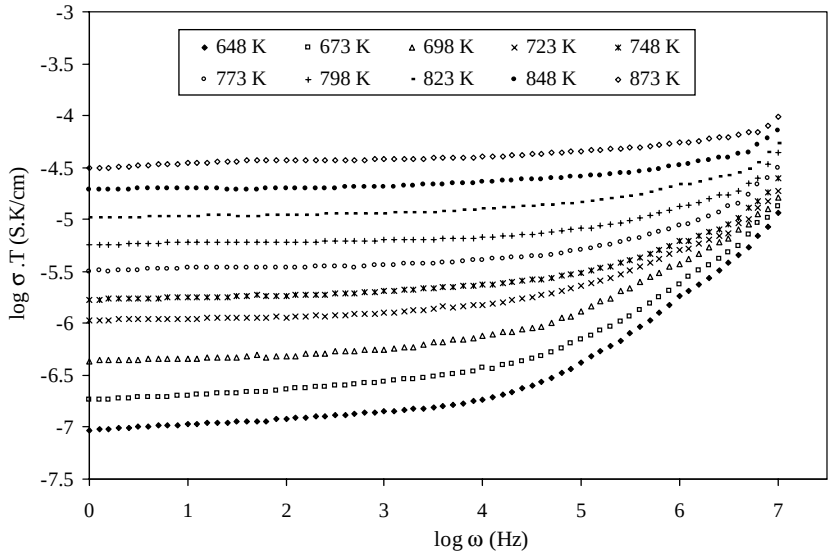

FIG. 4. Variation of conductivity vs frequency for $Na_2GaCd_2(PO_4)_3$ at different temperatures.

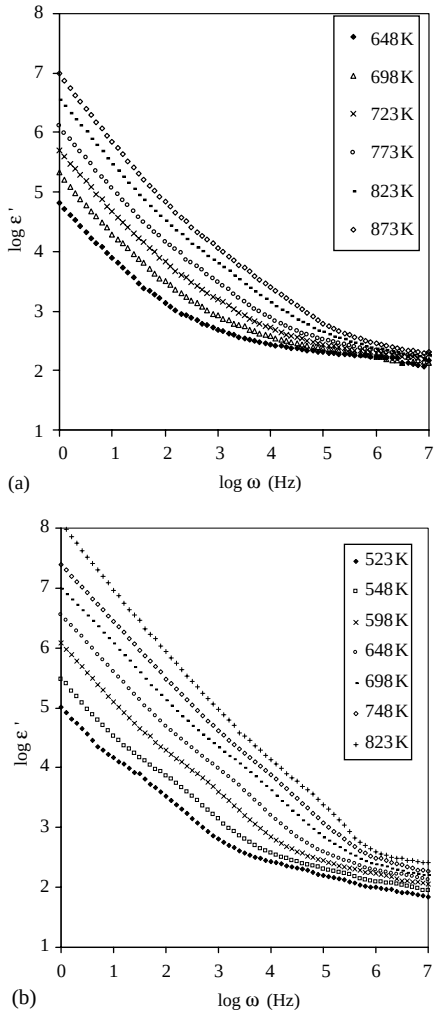

FIG. 5. Frequency dependence of the real parts of permittivity at different temperatures: (a) $Na_2GaCd_2(PO_4)_3$ and (b) $Na_2FeMnCd(PO_4)_3$.

narrow quasi-hexagonal windows (Fig. 10). The Na(2) sites are octahedrally surrounded by oxygen atoms (Fig. 9b) with mean distances ranging from ca. 2.48 Å for $GaCd_2$ to 2.65 Å for $InMn_2$, and the adjacent Na(2) positions are separated by wide hexagonal windows (Fig 10). It is worth noting that the Na(2) sites and the windows separating them are somewhat larger than the Na(1) ones. Taking into account the sums of the ionic radii $r_{Na^+} + r_{O^{2-}} \approx 2.40$ Å (26), likely diffusion can be assumed between the Na(2) position in all these compounds, because of the easy passageway formed by the large oxygen windows separating them (i.e., all the Na^+–O^{2-} distances are higher than the sums of Na^+ and O^{2-} radii, as stated above); whereas the diffusion of the Na(1) ions through the bottlenecks can be obstructed by the small size of the windows.

On the other hand, conductivities depend strongly on the electronic structure of the di- and trivalent ions (main or transition elements). The conductivity is higher when these ions are transition elements (27–29) and this fact is confirmed for the FeMnCd material (see Table 4).

The capacitance values from impedance measurements show the predominantly ionic nature of the conductivity in all these series. However, at low frequency incomplete semicircles of $GaMn_2$ and $InMn_2$ were inclined at $\sim 35^\circ$ to the real Z'-axis, suggesting some contribution of electronic conduction. This occurrence of mixed conduction can be confirmed by dc polarization/discharging studies.

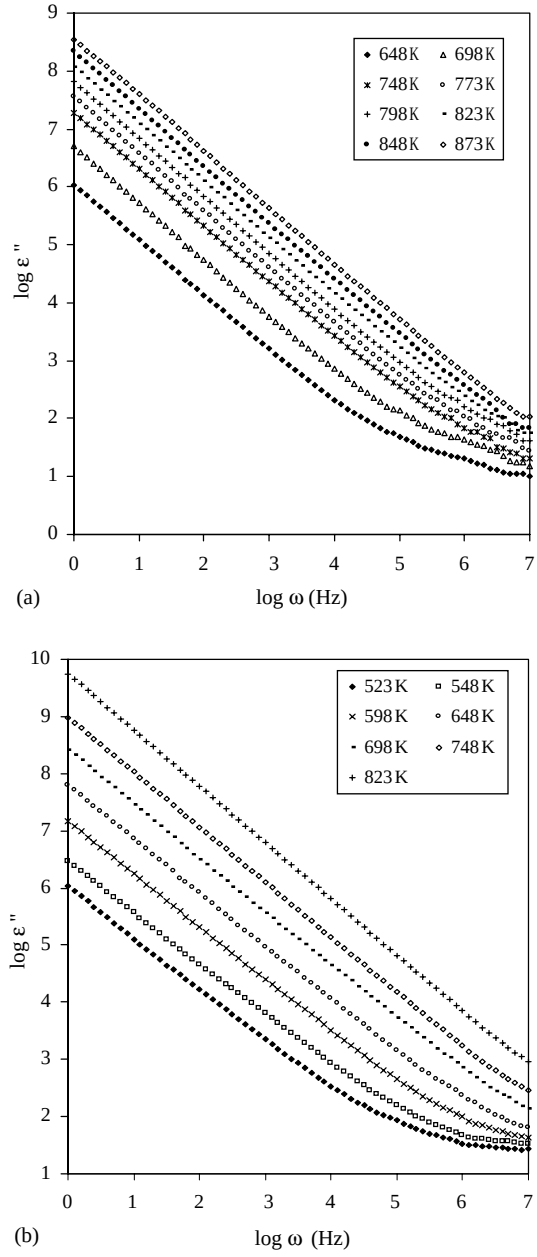

FIG. 6. Frequency dependence of the imaginary parts of permittivity at different temperatures: (a) $Na_2GaCd_2(PO_4)_3$ and (b) $Na_2FeMnCd(PO_4)_3$.

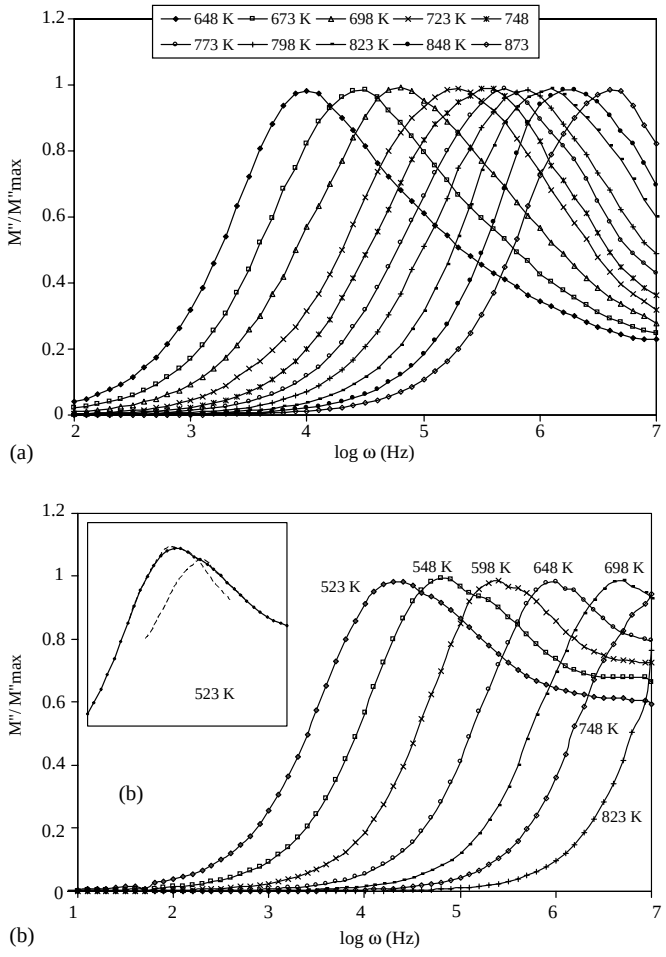

FIG. 7. Normalized modulus spectra for (a) $Na_2GaCd_2(PO_4)_3$ and (b) $Na_2FeMnCd(PO_4)_3$ the inset figure shows the unfolded peaks.

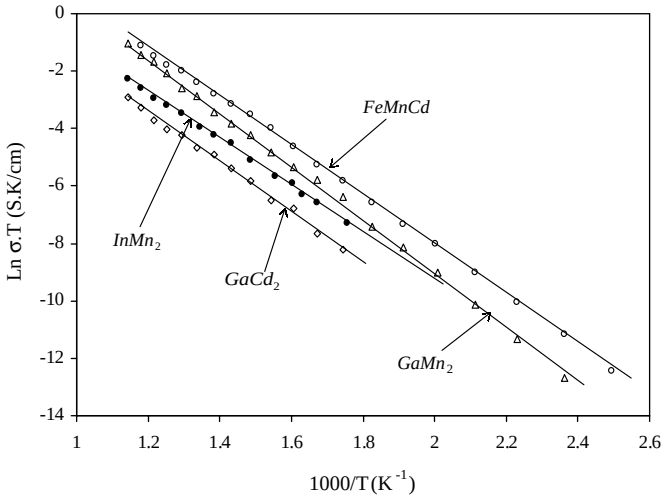

FIG. 8. Arrhenius conductivity plots.

TABLE 4
Unit-Cell Volumes, Activation Energies and Conductivities (S/cm) at Different Temperatures

	GaMn2	GaCd2	InMn2	FeMnCd
V (Å3)	891.19(3)	926.44(2)	940.64(4)	916.51(2)
E_a (eV)	0.81	0.75	0.71	0.75
σ 848 K) × 105	4.42	8.85	27.7	38.1
σ (798 K) × 105	2.27	5.11	16.0	21.2
σ (698 K) × 105	0.65	1.56	3.08	6.02
σ (673 K) × 105	0.43	0.91	2.21	4.44
σ (598 K) × 105	0.051	0.08	0.23	0.86

Polarization measurements. The polarization measurements, summarized in Fig. 11, were carried out in order to define the electronic and ionic contributions to the total conductivity. Charge/discharge experiments on cells consisting of pellets sandwiched between blocking platinum electrodes, showed that a significant amount of current could be passed on the charging cycle, but also a considerable amount of current could be detected in the discharge mode. This phenomenon can be explained by the fact that the products of charging were stored in the vicinity of the electrodes and were subsequently recovered on discharge, thereby indicating a certain contribution of ionic conduction.

The ratio $t = Q_d/Q_c$ (where Q_d and Q_c are the amount of charge passed in discharging and charging mode, respectively) gives an estimation of the ionic transport number. For purely ionic conductors, Q_d/Q_c should have the ideal value of unity. In a mixed ionic/electronic transport, this ratio gives an approximate estimation of the ionic transference number (30, 31).

In the case of $GaCd_2$ (Fig. 11a), no electronic contribution can be detected taking into account that the Cd^{II} and Ga^{III} have d^{10} electron configuration. On the other hand, the response of charge/discharge cycles of FeMnCd is quite similar to that of $GaCd_2$, suggesting that they have the

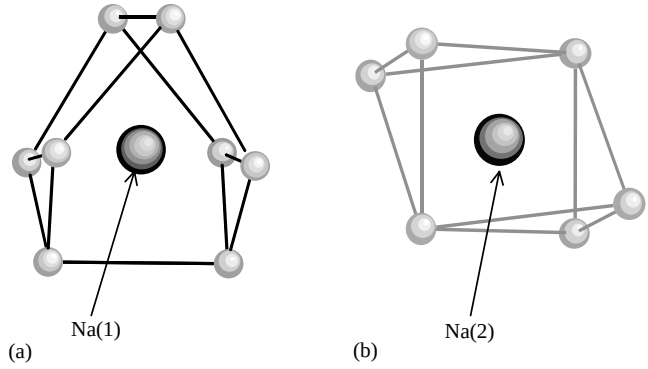

FIG. 9. Coordination polyhedra of the sodium atoms: (a) Na(1) and (b) Na(2).

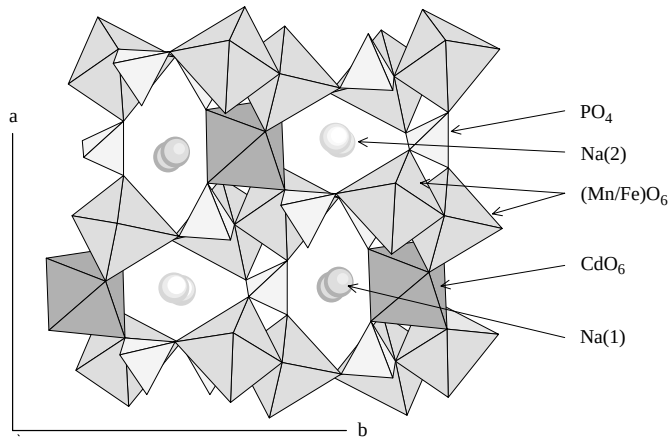

FIG. 10. Projection of the structure of $Na_2FeMnCd(PO_4)_3$ along the *ab* plane showing the windows separating the adjacent Na cations.

same electrical behavior. Therefore, the electrical response in these two cadmium-containing phases is only due to the alkaline cation mobility. By contrast, the experimental data of $GaMn_2$ (Fig. 11b), which is quite similar to that of $InMn_2$, indicate some discharge efficiency, and the results seem to confirm a mixed electronic–ionic conduction behavior in these two latter materials.

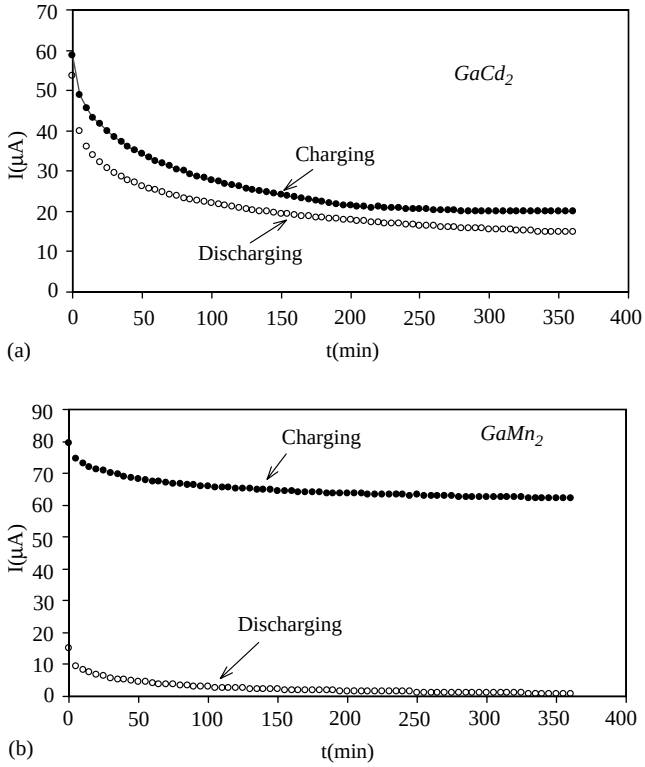

FIG. 11. Current vs time for charging/discharging cycles for (a) $Na_2GaCd_2(PO_4)_3$ and (b) $Na_2GaMn_2(PO_4)_3$ samples at 723 K and with a charging voltage of 0.5 V.

Magnetic Behaviour

The magnetic measurements were carried out for the three Mn-containing compounds and in Fig. 12 are depicted the molar susceptibility results and their reciprocal for FeMnCd (a) and $InMn_2$ (b), that show the same trend as $GaIn_2$. These data can be fitted to the Curie–Weiss equation $\chi_M = C/(T-\theta)$ in a wide temperature range and the yielded C, θ and μ_B values are gathered in Table 5. Experimental magnetic moments agree well with the expected values for Mn^{2+} and/or Fe^{3+} in high spin states.

The negative value of θ together with the continuous increase of χ_M with decreasing T may arise from antiferromagnetic exchanges as major interaction between adjacent Fe–Mn or Mn–Mn ions. At low temperature, the deviation of $1/\chi_M$ from the Curie–Weiss linear variation to larger values, however, suggests the presence of a magnetic phase transition below the critical temperature T_C (Table 5). This fact indicates the possible presence of some weak ferromagnetic contributions in these compounds.

The magnetic behavior of these phases is quite similar to that observed in the isostructural $Ag_2FeMn_2(PO_4)_3$ compound (5). However, the spin coupling within the $(FeMnCdO_{12})_\infty$, $(GaMn_2O_{12})_\infty$ or $(InMn_2O_{12})_\infty$, chains

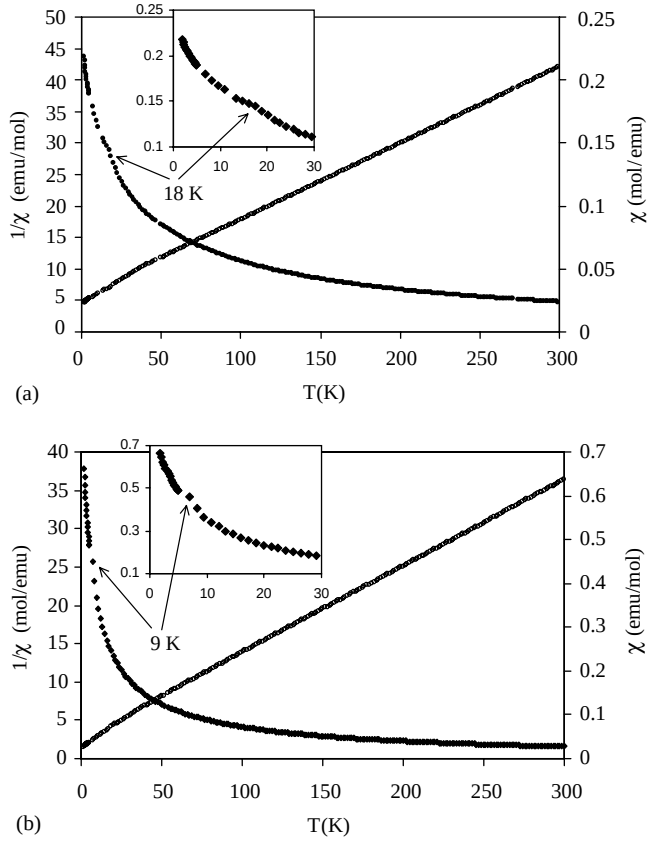

FIG. 12. Molar and inverse molar magnetic susceptibility data for (a) $Na_2FeMnCd(PO_4)_3$ and (b) $Na_2InMn_2(PO_4)_3$ in an applied field of 500 G.

TABLE 5
Magnetic Data for $Na_2FeMnCd(PO_4)_3$ and $Na_2InMn_2(PO_4)_3$ Compounds

Compounds	Temperature range of fitted data (K)	C (g K/mol)	θ (K)	μ_{exp} (μB)	μ_{cal} (μB)	T_C (K)
FeMnCd	300–30	8.33	–24.3	8.16	8.37	18
$InMn_2$	300–20	8.94	–11.6	8.46	8.37	9
$GaMn_2$	300–20	8.90	–11.0	8.40	8.37	10

is significantly weakened by the presence of diamagnetic Cd, Ga or In ions, respectively.

These results allow to conclude that new sodium orthophosphates with the alluaudite structures (Special group $C2/c$) have been synthesized, using solid-state reactions. Their electrical properties have been determined by impedance spectroscopy and polarization measurements. These solid electrolytes are Na^+ ion conductors due to the presence of these cations in the tunnels along the c-axis. The activation energies deduced for each compound show that the conductivity increases with increasing unit-cell volumes and this fact is interpreted in terms of the size relation between the mobile cations and the bottleneck of the diffusion pathway. On the other hand, the charging/discharging measurements suggest that GaMn and $InMn_2$ possess an electronic contribution to the electrical conductivity while $GaCd_2$, and FeMnCd are purely ionic conductors.

The magnetic measurements reveal the antiferromagnetic nature of the interactions between adjacent Fe–Mn or Mn–Mn ions, although at low temperatures some weak ferromagnetic contributions are observed.

ACKNOWLEDGMENTS

Financial support from CICYT, Spain (Grant MAT2000-1585-C03-02) is gratefully acknowledged. The authors thank Dr. A. Santrich, I.C.M.M., C.S.I.C, for magnetic measurements.

REFERENCES

1. D. J. Fisher, *Am. Mineral.* **40,** 1100 (1955).
2. P. B. Moore, *Am. Mineral.* **56,** 1955 (1971).
3. D. Antenucci, A. M. Fransolet, G. Miehe, and P. Tarte, *Eur. J. Mineral.* **7,** 175 (1995).
4. M. B. Korzenski, G. L. Schimek, and J. W. Kolis, *J. Solid State Chem.* **139,** 152 (1998).
5. N. Chouaibi, A. Daidouh, C. Pico, A. Santrich, and M. L. Veiga, *J. Solid State Chem.* **159,** 46 (2001).
6. A. Daidouh, C. Durio, C. Pico, M. L. Veiga, N. Chouaibi, and A. Ouassini, *Solid State Sci.* **4,** 541 (2002).
7. F. D'Yvoire and F. Réme, *C. R. Acad. Sci. Paris* **290,** 185 (1980).
8. S. Khorari, A. Rulmount, R. Cahay, and P. Tarte, *J. Solid State Chem.* **118,** 267 (1995).
9. S. Khorari, A. Rulmount, and P. Tarte, *J. Solid State Chem.* **134,** 31 (1997).
10. T. E. Warner, W. Milius, and J. Maier, *J. Solid State Chem.* **106,** 301 (1993).
11. F. D'Yvoire, E. Bretey, and G. Collin, *Solid State Ionics* **28–30,** 1259 (1988).
12. J. Rodriguez-Carvajal, Fullprof Program for Rietveld Refinement, an pattern machine analysis, "Satellite Meeting on Powder Diffraction, XVth Conference of International Union of Crystallography," Toulouse, p. 127, 1998.
13. A. Laghzizil, A. Bouhaouss, M. Ferhat, P. Barboux, R. Morineau, and J. Livage, *Solid State Ionics* **67,** 137 (1993).
14. B. Orgaz and A. Huanosta, *J. Solid State Chem.* **97,** 65 (1992).
15. K. S. Cole and R. H. Cole, *J. Chem. Phys.* **9,** 341 (1941).
16. A. K. Jonscher, "Dielectric Relaxation in Solids." Chelsea Dielectric Press, London, 1996.
17. J. Fleig and J. Maier, *J. Electrochem. Soc.* **145,** 2081 (1997).
18. A. I. Ruiz, M. L. López, M. L. Veiga, and C. Pico, *Solid State Ionics* **112,** 291 (1998).
19. J. R. MacDonald, "Impedance Spectroscopy: Emphasizing Solid Materials and Systems." Wiley-Interscience, New York, 1987.
20. C. Cramer, K. Funke, T. Saatkamp, D. Wilmer, and M. D. Ingram, *Z. Naturforsch.* **50,** 613 (1995).
21. K. Funke, *Solid State Ionics* **28–30,** 100 (1988).
22. A. K. Jonscher, *Nature* **264,** 673 (1977).
23. A. Daidouh, M. L. Veiga, and C. Pico, *Solid State Ionics* **106,** 103 (1998).
24. A. Daidouh, C. Pico, and M. L. Veiga, *Solid State Ionics* **124,** 109 (1999).
25. R. J. Grant, Y. M. Hodge, M. D. Ingram, and A. R. West, *J. Am. Ceram. Soc.* **60,** 226 (1977).
26. R. D. Shannon, *Acta Crystaollgr. A* **32,** 751 (1976).
27. J. M. Winard, A. Rulmont, and P. Tarte, *J. Solid State Chem.* **107,** 356 (1993).
28. J. M. Winard, A. Rulmont, and P. Tarte, *J. Solid State Chem.* **93,** 341 (1993).
29. J. M. Winard, A. Rulmont, and P. Tarte, *J. Mater. Sci.* **25,** 4008 (1990).
30. H. H. Sumathipala, M. A. K. L. Dissanayake, and A. R. West, *J. Electrochem. Soc.* **142**(7), 2138 (1995).
31. A. I. Ruiz, M. L. López, M. L. Veiga, and C. Pico, *Eur. J. Inorg. Chem.* **4,** 659 (2000).